

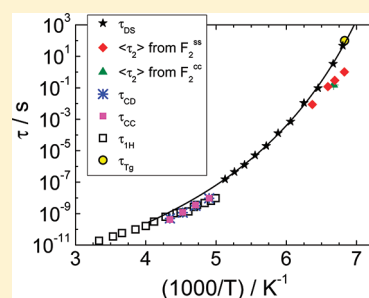
# Secondary Water Relaxation in a Water/Dimethyl Sulfoxide Mixture Revealed by Deuteron Nuclear Magnetic Resonance and Dielectric Spectroscopy

S. A. Lusceac,<sup>†</sup> C. Gainaru,<sup>‡</sup> D. A. Ratzke,<sup>†</sup> M. F. Graf,<sup>†</sup> and M. Vogel<sup>\*,†</sup>

<sup>†</sup>Institut für Festkörperphysik, Technische Universität Darmstadt, Hochschulstrasse 6, 64289 Darmstadt, Germany

<sup>‡</sup>Fakultät für Physik, Technische Universität Dortmund, 44221 Dortmund, Germany

**ABSTRACT:** We exploit the potential of a combined dielectric spectroscopy (DS) and deuteron nuclear magnetic resonance (<sup>2</sup>H NMR) approach to investigate the molecular dynamics in a supercooled 2:1 molar mixture of deuterated water (D<sub>2</sub>O) and dimethyl sulfoxide (DMSO). While DS probes the rotational motion of both components, application of <sup>2</sup>H NMR allows us to single out the dynamical behavior of the water molecules. Combining the results of both methods, we can follow the slowdown of the  $\alpha$ -process of the mixture over more than 10 orders of magnitude in time, revealing that the Vogel–Fulcher–Tammann (VFT) equation describes well its temperature dependence down to the glass transition temperature,  $T_g = 146$  K. While the <sup>2</sup>H NMR data do not provide evidence for a secondary relaxation process in the weakly supercooled regime, they indicate that, in the deeply supercooled regime,  $T_g \leq T \leq 160$  K, the water molecules do show a secondary dynamical process, which is faster and exhibits a weaker temperature dependence than the  $\alpha$ -process of the mixture. Consistently, the shape of the dielectric spectra changes in this temperature range. <sup>2</sup>H NMR rotational correlation functions reveal that this faster secondary water process destroys essentially all orientational correlation. In addition, these data show that the water reorientation process is characterized by a mean elementary jump angle smaller than 13°. Possible origins of the faster secondary water process in the deeply supercooled mixture are discussed.



## INTRODUCTION

Water plays an essential role in human life, and the world as we know it would be totally different without it. For many different materials, the presence of water dictates the material properties and, hence, it is important to investigate and to understand the behavior of water in these systems. For example, water is an important ingredient in construction materials, food products, drugs, chemical reactants, and so on. Moreover, the physiological functions of proteins depend on the presence of a hydration layer. While a number of researchers believe that water exhibits universal dynamical properties in various environments,<sup>1–3</sup> the nature of water dynamics is still a matter of controversial debate, in particular, for water in confinements and mixtures.<sup>1–11</sup>

In neutron scattering works on protein hydration waters, a sharp fragile-to-strong dynamic crossover for the hydration water of lysozyme was attributed to a transition between high-density and low-density forms of liquid water at about 220 K,<sup>7</sup> while other workers argued, based on results for water in the hydration shell of C-phycocyanin, that any dynamic discontinuity at this temperature can be ruled out when using an improved data analysis.<sup>12</sup> Moreover, dielectric spectroscopy (DS) studies found no evidence for the existence of a sharp fragile-to-strong transition for the hydration waters of several proteins at ca. 220 K.<sup>2,4,11,13</sup> However, for various aqueous binary glass formers, in particular for mixtures of water with low-molecular weight compounds, a mild crossover from non-Arrhenius to Arrhenius

temperature dependence of water dynamics was found to occur upon cooling through the respective calorimetric glass transition temperature  $T_g$  of the mixture.<sup>1–3</sup>

Recently, we showed that DS and NMR yield consistent results for the temperature-dependent correlation times of water reorientation in the hydration shell of proteins.<sup>14–16</sup> For the hydration waters of elastin and collagen, application of both methods revealed Arrhenius behavior in the temperature range 130–270 K, i.e., below the glass transition or denaturation temperatures of these proteins. Furthermore, we exploited the fact that <sup>2</sup>H NMR enables detailed insights into not only the time constants, but also the mechanism for water rotational motion.<sup>14–16</sup> The analysis showed that, near ambient temperatures, long-range water diffusion is associated with isotropic rotational motion on a time scale shorter than microseconds. However, below about 220 K, the mechanisms for the rotational motion on a time scale of microseconds and milliseconds differ for the hydration waters of various proteins. Specifically, a pronounced anisotropy was observed for the reorientation of water in the hydration shell of myoglobin,<sup>14,15</sup> while any anisotropy, if existent, is weak in the hydration shells of elastin and collagen.<sup>16</sup>

**Received:** July 6, 2011

**Revised:** August 30, 2011

**Published:** August 31, 2011

Motivated by these findings for the dynamics of water in mixtures with proteins, we use a combination of DS and NMR to study the rotational motion of water in a glass-forming mixture with a low-molecular weight compound. Specifically, we investigate a 2:1 molar mixture of D<sub>2</sub>O and dimethyl sulfoxide (DMSO). Thus, the second component is much more mobile in the present aqueous mixture than in the previously studied water–protein mixtures, and the chemical and topological environments of the water molecules are different, allowing us to compare water dynamics in very diverse environments and to address the question of the universality of the dynamical behavior of water. In addition, the studied D<sub>2</sub>O/DMSO mixture is a model system for binary glass formers comprised of low-molecular weight compounds. While DS probes the rotational motion of both components of the mixture, <sup>2</sup>H NMR provides us with the opportunity to separately investigate the water dynamics. In particular, we exploit the fact that <sup>2</sup>H NMR allows us to determine both the time scale and the mechanism for the rotational motion of water.

## THEORETICAL BACKGROUND AND DATA ANALYSIS

Molecular reorientation processes can be described via the rotational autocorrelation functions  $f_l(t) = \langle P_l[\cos \theta(0)]P_l[\cos \theta(t)] \rangle / \langle P_l[\cos \theta(0)]^2 \rangle$ . Here, the brackets  $\langle \dots \rangle$  denote the ensemble average,  $P_l$  is the Legendre polynomial of rank  $l$ , and  $\theta$  is an angle describing the molecular orientation.

**Dielectric Spectroscopy.** DS probes the reorientation of electric dipoles, as described by the autocorrelation function  $f_1(t)$ .<sup>17</sup> The dielectric response is usually recorded in the form of the complex dielectric permittivity  $\varepsilon^*(\omega) = \varepsilon'(\omega) - i\varepsilon''(\omega)$ . The imaginary part, the dielectric loss  $\varepsilon''(\omega)$ , is related to the Fourier transform of  $f_1(t)$  via  $\varepsilon''(\omega) = \omega \Delta \varepsilon \text{Re}\{F[f_1(t)]\}$ . Here,  $\Delta \varepsilon = \varepsilon_i - \varepsilon_\infty$  is the relaxation strength, with  $\varepsilon_i$  and  $\varepsilon_\infty$  being the values of the dielectric constant at sufficiently low and high frequencies, respectively.

If the reorientation process is characterized by a single correlation time  $\tau$ , i.e.,  $f_1(t) = \exp(-t/\tau)$ , the dielectric loss is given by the Debye equation,<sup>17</sup>  $\varepsilon'' = \Delta \varepsilon \omega \tau / (1 + \omega^2 \tau^2)$ . For supercooled liquids, the dielectric response is usually not monodispersive. Here, we fit the data to the empiric Havriliak–Negami (HN) relation,<sup>18</sup>  $\varepsilon''(\omega) = \Delta \varepsilon \text{Im}[1 + (i\omega\tau)^\alpha]^{-\gamma}$ . This function gives rise to  $\omega^{\alpha+\gamma}$  and  $\omega^{-\alpha\gamma}$  dependencies of the low- and the high-frequency flanks of the dielectric loss peak, respectively, and reduces to the Cole–Cole (CC) relation for  $\gamma = 1$ , to the Cole–Davidson (CD) relation for  $\alpha = 1$ , and to the Debye form for  $\alpha = \gamma = 1$ .

**<sup>2</sup>H NMR.** In the present <sup>2</sup>H NMR experiments, we probe the quadrupolar frequency  $\omega_Q$  of the water deuterons, which is approximately given by<sup>19</sup>

$$\omega_Q = \frac{1}{2} \delta [3 \cos^2(\theta) - 1] \propto P_2[\cos(\theta)] \quad (1)$$

Here,  $\theta$  is the angle between the axis of the O–<sup>2</sup>H bond and the direction of the external static magnetic field. The anisotropy parameter  $\delta$  describes the strength of the quadrupolar interaction of the water deuterons. For the present analyses, we use  $\delta = 2\pi \cdot 164.8$  kHz, as determined from the <sup>2</sup>H NMR line shape at sufficiently low temperatures.

For isotropic reorientation, the <sup>2</sup>H spin–lattice relaxation time  $T_1$  is related to the spectral density of the rotational motion,

$J(\omega)$ , according to<sup>20,21</sup>

$$\frac{1}{T_1} = \frac{2}{15} \delta^2 [J(\omega_0) + 4J(2\omega_0)] \quad (2)$$

$J(\omega)$  is obtained from the autocorrelation function  $f_2(t)$  via Fourier transformation. In the case of an exponential correlation function,  $f_2(t) = \exp(-t/\tau)$ , the Debye spectral density results in

$$J_D(\omega) = \frac{\tau}{1 + (\omega\tau)^2} \quad (3)$$

Then, spin–lattice relaxation analysis provides straightforward access to the correlation time  $\tau$  of the motion. However, for complex molecular dynamics, as found in supercooled liquids, the correlation functions are nonexponential, and determination of the time scale of molecular dynamics requires knowledge about the shape of the underlying distribution  $G(\log \tau)$ . In the past, the CC and CD spectral densities proved useful to describe complex molecular dynamics.<sup>21,22</sup> For example, the  $J_{CC}$  spectral density was found to be suitable to describe the dynamics of protein hydration waters,<sup>14</sup> while the  $J_{CD}$  spectral density was usually employed to analyze molecular reorientation in neat glass-forming liquids.<sup>23,24</sup> The CC spectral density, which is associated with a symmetric distribution  $G(\log \tau)$ , reads<sup>22</sup>

$$J_{CC}(\omega) = \frac{\sin\left(\frac{\pi}{2}\beta_{CC}\right)(\omega\tau_{CC})^{\beta_{CC}}}{\omega \left[1 + (\omega\tau_{CC})^{2\beta_{CC}} + 2\cos\left(\frac{\pi}{2}\beta_{CC}\right)(\omega\tau_{CC})^{\beta_{CC}}\right]} \quad (4)$$

Here,  $\tau_{CC}$  is the position of the maximum of  $G(\log \tau)$  and  $\beta_{CC}$  is the width parameter. For asymmetric distributions  $G(\log \tau)$ , the CD spectral density<sup>22</sup>

$$J_{CD}(\omega) = \frac{\sin[\beta_{CD} \arctan(\omega\tau)]}{\omega[1 + (\omega\tau)^2]^{\beta_{CD}/2}} \quad (5)$$

is widely used, where  $\beta_{CD}$  is the width parameter. In this case, the mean correlation time  $\tau_{CD}$  can be obtained via  $\tau_{CD} = \tau\beta_{CD}$ .

For molecular dynamics in the milliseconds time range, application of the stimulated-echo pulse sequence, pulse- $t_1$ –pulse- $t_m$ –pulse- $t_2$ , enables direct measurement of rotational autocorrelation functions.<sup>19,21</sup> Here,  $t_1$  is referred to as the evolution time,  $t_m$  is the mixing time, and  $t_2$  is the detection time. This pulse sequence generates a stimulated echo at a detection time  $t_2 = t_1 \equiv t_p \ll t_m$ . When using appropriate lengths and phases of the pulses, the rotational autocorrelation functions<sup>19,21</sup>

$$F_2^{cc}(t_m, t_p) = \frac{\langle \cos[\omega_Q(0)t_p] \cos[\omega_Q(t_m)t_p] \rangle}{\langle \cos[\omega_Q(0)t_p] \cos[\omega_Q(0)t_p] \rangle} \quad (6)$$

$$F_2^{ss}(t_m, t_p) = \frac{\langle \sin[\omega_Q(0)t_p] \sin[\omega_Q(t_m)t_p] \rangle}{\langle \sin[\omega_Q(0)t_p] \sin[\omega_Q(0)t_p] \rangle} \quad (7)$$

can be obtained from observation of the stimulated-echo height for various values of  $t_m$  and a constant value of  $t_p$ . Here, we assume that molecular dynamics during the evolution and detection times can be neglected ( $\tau \gg t_p$ ). Note that, in the limit  $t_p \rightarrow 0$ ,  $F_2^{ss}(t_m) \approx f_2(t_m)$  since  $\sin(\omega_Q t_p) \approx \omega_Q t_p \propto P_2(\cos \theta)$ .

In general,  $F_2^{cc}(t_m)$  and  $F_2^{ss}(t_m)$  decay to a plateau  $F_\infty^{xx}$  ( $x = c, s$ ), the height of which depends on the geometry of the motion and

on the value of  $t_p$ . Moreover, in addition to molecular dynamics, spin–lattice relaxation acts during the mixing time and damps the stimulated echo. Therefore, we fit the data with the function

$$F_2^{xx}(t_m, t_p) = \left\{ [1 - F_\infty^{xx}(t_p)] \exp \left[ - \left( \frac{t_m}{\tau^x(t_p)} \right)^{\beta^x(t_p)} \right] + F_\infty^{xx}(t_p) \right\} \exp \left[ - \left( \frac{t_m}{T_{SLR}} \right)^{\beta_{SLR}} \right] \quad (8)$$

In doing so, we considered that the decays due to both molecular dynamics and spin–lattice relaxation are usually well described by Kohlrausch–Williams–Watts (KWW) functions.<sup>25</sup> On the basis of the fit parameters  $\tau^x$  and  $\beta^x$ , mean rotational correlation times can be calculated according to

$$\langle \tau^x(t_p) \rangle = \frac{\tau^x(t_p)}{\beta^x(t_p)} \Gamma \left( \frac{1}{\beta^x(t_p)} \right) \quad (9)$$

with  $\Gamma$  denoting the Gamma function. The angles of the elementary rotational jumps of a molecular reorientation process can be determined when analyzing  $\langle \tau^x \rangle$  as a function of  $t_p$ .<sup>19,21</sup> For large-angle jumps,  $\langle \tau^x \rangle$  is virtually independent of the value of  $t_p$ , while for small-angle jumps the time constants decrease by orders of magnitude with decreasing  $t_p$ .

Strictly speaking, the spin–lattice relaxations of Zeeman and alignment orders are relevant in measurements of  $F_2^{cc}$  and  $F_2^{ss}$ , respectively. While the decay of the alignment order cannot be measured independently, it is possible to determine the former in a regular spin–lattice relaxation experiment. Therefore, we performed spin–lattice relaxation measurements, fitted the resulting relaxation functions to a KWW function to determine the relaxation time  $T_1$  as well as the stretching parameter  $\beta_{T1}$ , and kept the values  $T_{SLR} = T_1$  and  $\beta_{SLR} = \beta_{T1}$  fixed when analyzing the decays of  $F_2^{cc}$  to reduce the number of free parameters. To fit the  $F_2^{ss}$  data, we also used the constraints  $T_{SLR} = T_1$  and  $\beta_{SLR} = \beta_{T1}$ , exploiting the fact that the spin–lattice relaxation time of the alignment state, although shorter, is still on the same order of magnitude as that of the Zeeman state for amorphous samples with  $T_1 \leq 1$  s.<sup>26–29</sup> In general, neglecting the different relaxation behavior of Zeeman and alignment orders may render determination of correlation times from  $F_2^{ss}$  ambiguous. Below, we will demonstrate by comparison of results from  $F_2^{ss}$  and  $F_2^{cc}$  that reliable results can be obtained from the former correlation functions for the studied sample and temperature range. In addition, we used the parameters  $T_1$  and  $\beta_{T1}$  obtained from the spin–lattice relaxation measurements to calculate mean spin–lattice relaxation times  $\langle T_1 \rangle$  in analogy with eq 9.

## MATERIALS AND EXPERIMENTAL DETAILS

DMSO and D<sub>2</sub>O were purchased from Merck (99% purity) and from Aldrich (99.9% <sup>2</sup>H atom purity), respectively. Both liquids were used as received. The D<sub>2</sub>O/DMSO mixture was prepared in a 2:1 molar ratio by weighing.

The dielectric investigations were performed in a frequency range  $10^{-3}$  Hz  $< \nu < 10^7$  Hz using a broadband  $\alpha$ -spectrometer from Novocontrol. The sample was placed between two parallel plates of a capacitor built for investigations of liquid materials in analogy with the one described in a previous study.<sup>30</sup> The empty cell had a geometric capacitance of about 20 pF. The capacitor filled with the material was inserted into a Novocontrol cryostat,

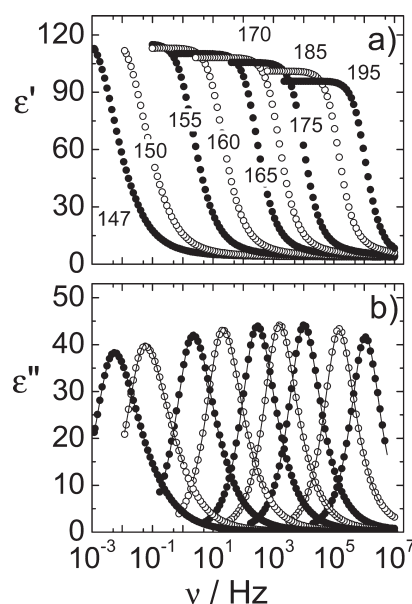


**Figure 1.** Real (a) and imaginary (b) parts of the complex dielectric permittivity  $\epsilon^*(\omega)$  of the 2:1 molar D<sub>2</sub>O/DMSO mixture. The numbers indicate temperatures in Kelvin. In panel b, the solid lines are HN interpolations of the dielectric loss peaks.

where the temperature was stabilized within 0.2 K by a Quatro controller. DS is sensitive to the dynamics of both components of the mixture as they have comparable dipole moments<sup>31,32</sup> ( $\mu_{\text{DMSO}} = 3.96 \pm 0.40$  D,  $\mu_{\text{D}_2\text{O}} = 1.8506 \pm 0.0021$  D).

For the NMR studies, the sample was degassed and flame-sealed in a 5 mm diameter Wilmad NMR glass tube. The experiments were performed using a home-built NMR spectrometer. The associated Oxford superconducting magnet provides a field of about 7 T, corresponding to a <sup>2</sup>H Larmor frequency of  $\omega_0 = 2\pi \times 46.1$  MHz. The home-built probe was placed into a Konti CryoVac cryostat operated with liquid nitrogen and controlled by a TIC 304 MA CryoVac temperature controller. The setup enabled long-time temperature stability better than 1 K.

The spin–lattice relaxation measurements were performed using the inversion–recovery method in the temperature range 204–230 K and the saturation–recovery method at lower temperatures. In stimulated-echo experiments, we utilized a four-pulse sequence with a minimum phase cycle of 16 steps.<sup>33</sup> The fourth pulse was employed to overcome the dead time of the receiver and applied after a delay of 20  $\mu$ s. The length of the 90° pulses was 2.1  $\mu$ s, ensuring proper excitation of the broad <sup>2</sup>H NMR spectrum.

## RESULTS

**Dielectric Spectroscopy Studies.** Figure 1 presents the dielectric response of the studied 2:1 molar D<sub>2</sub>O/DMSO mixture at various temperatures. A strong relaxation process enters the accessible frequency window at about 200 K and shifts toward lower frequencies with decreasing temperature. Due to large dipole moments of both DMSO and D<sub>2</sub>O molecules,<sup>31,32</sup> the dielectric response contains contributions from both components. This explains the large static permittivity  $\epsilon_s$  observed for the studied mixture. The values of  $\epsilon_i$  and  $\epsilon_\infty$  can be directly accessed from the limits of the low- and high-frequency plateaus of  $\epsilon'(\omega)$  (see Figure 1a), revealing a temperature independent value of  $\epsilon_\infty \approx 4$ . Upon cooling, the



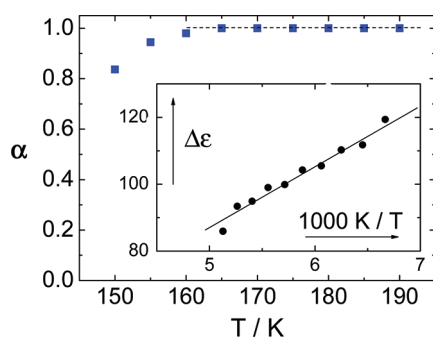


**Figure 2.** Results of HN fits to the dielectric loss peaks in Figure 1b. The dashed line marks  $\alpha = 1$ . The inset shows the relaxation strength  $\Delta\epsilon$  as a function of the inverse temperature. The solid line is an interpolation with a Curie law:<sup>17</sup>  $\Delta\epsilon = (17500 \pm 100) \text{ K}/T$ .

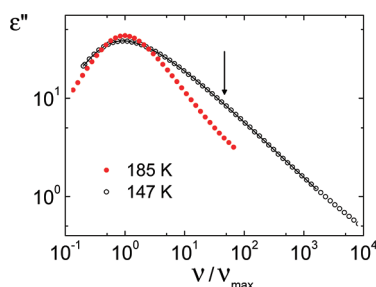


**Figure 3.** Dielectric spectra recorded at 147 and 185 K. To enable straightforward comparison of the spectral shape, the data are shown on a scaled frequency axis  $\nu/\nu_{\text{max}}$ , where  $\nu_{\text{max}}$  is the position of the peak maximum. The solid line is a fit of the data at  $T = 147 \text{ K}$  with two HN functions. The arrow indicates the accordingly scaled rate of the dynamic process observed in NMR at this temperature. When fitting the DS data at  $T = 147 \text{ K}$  with two HN functions, the parameter  $\tau$  of the faster process was fixed at the indicated value of the time constant obtained from NMR.

relaxation strength  $\Delta\epsilon(T) = \epsilon_i(T) - \epsilon_\infty$  of the mixture continuously increases in a Curie-like fashion typical of the  $\Delta\epsilon(T)$  evolution in supercooled molecular liquids<sup>17</sup> (see below).

The relaxation strength is also reflected by the area under the loss peaks in Figure 1b since  $\Delta\epsilon = (2/\pi) \int \epsilon''(\omega) d \ln(\omega)$ . If the shape of  $\epsilon''(\omega)$  does not vary much with temperature, the temperature dependence of the peak height  $\epsilon''_{\text{max}}$  will follow that of  $\Delta\epsilon$ . Upon cooling, we observe that  $\epsilon''_{\text{max}}$ , like  $\Delta\epsilon$ , increases for  $T$  down to ca. 170 K, implying that frequency–temperature superposition applies to a good approximation in this range. However, when the temperature is further decreased, the peak height decreases, i.e.,  $\epsilon''_{\text{max}}$  is a maximum at  $T \approx 170 \text{ K}$ , indicating a crossover in the spectral evolution at this temperature. Since  $\Delta\epsilon(T)$  does not show such maximum (see Figure 1a), this crossover results from changes of the spectral shape and, thus, of the dynamics of the system. Specifically, the decrease of  $\epsilon''_{\text{max}}$  reflects a broadening of the loss curves below 170 K.

In order to quantify this model-independent finding, we interpolate the loss peaks with a HN function. The fit quality is excellent for all temperatures, except the lowest one,  $T = 147 \text{ K}$  (see Figure 1b). Inspecting the inset of Figure 2, it is evident that the fit parameter  $\Delta\epsilon$  obeys the Curie law for  $195 \text{ K} > T > 150 \text{ K}$ ,

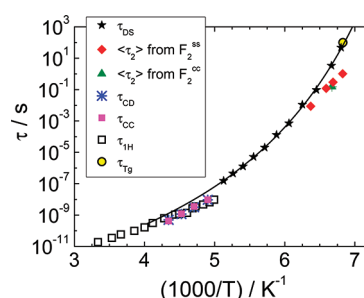


**Figure 4.** Correlation times:  $\tau_{\text{DS}}$  from DS experiments;  $\langle\tau_2\rangle$  from NMR correlation functions;  $\tau_{\text{CD}}$  from a CD fit of the spin–lattice relaxation times;  $\tau_{\text{CC}}$  from a CC fit of the spin–lattice relaxation times;  $\tau_{\text{Tg}}$ : time set to 100 s at the glass transition temperature (from DSC experiments<sup>37</sup>);  $\tau_{\text{1H}}$  from analysis of the  $^1\text{H}$  NMR spin–lattice relaxation times of a similar mixture.<sup>38</sup> Solid line: VFT fit of  $\tau_{\text{DS}}$ .

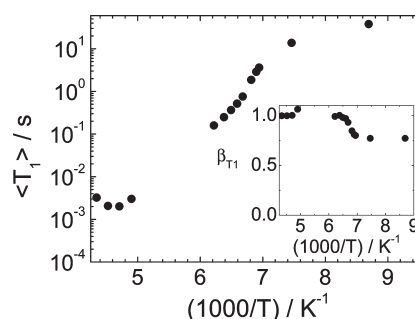


**Figure 5.** Mean  $^2\text{H}$  spin–lattice relaxation times  $\langle T_1 \rangle$  as a function of inverse temperature. Inset: stretching parameter  $\beta_{\text{T1}}$  characterizing the nonexponentiality of the  $^2\text{H}$  spin–lattice relaxation function.

consistent with the above-mentioned observations for  $\epsilon'(\omega)$ . Moreover, the time constant  $\tau$  follows the Vogel–Fulcher–Tammann (VFT) equation in this temperature range, vide infra. However, the temperature dependence of the shape parameter  $\alpha$  clearly changes at about 165 K. In Figure 2, we see that, above 165 K,  $\alpha$  could be kept fixed at  $\alpha = 1$ , while the good quality of the fits is maintained only if this parameter is unconstrained below this temperature. In the latter range,  $\alpha$  decreases upon cooling, indicating that the observed molecular relaxation processes are spread over a wider frequency range at lower temperatures, consistent with our conclusions based on  $\epsilon''_{\text{max}}(T)$ .

To further ascertain this change of the spectral shape, dielectric spectra at 147 and 185 K, i.e., below and above the crossover temperature,  $T \approx 170 \text{ K}$ , are compared in Figure 3. The spectra are shown on a scaled frequency axis, enabling straightforward comparison of their shapes. It is evident that the spectrum at 147 K is substantially broadened. A more careful inspection of this spectrum reveals a shoulder on the high-frequency flank of the main peak so that it cannot be described by a single peak function. Consequently, a sum of two HN functions was used to interpolate this spectrum. Since a free fitting procedure did not converge, as the two processes are close to each other and, thus, difficult to disentangle, we fixed the parameter  $\tau$  of the faster process to the value obtained from our NMR experiments (see below). Using this constraint, a stable fit resulted, which is shown in Figure 3. In Figure 4, the dielectric

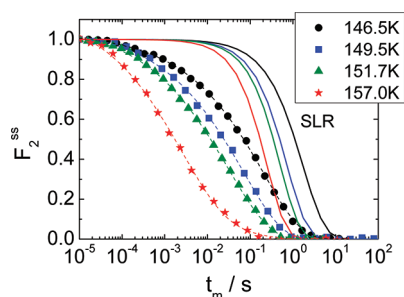


**Figure 6.** Correlation functions  $F_2^{ss}(t_m)$  for an evolution time  $t_p = 3 \mu\text{s}$  at various temperatures. The data are normalized to the value at the shortest mixing time  $t_m = 10^{-5} \text{ s}$ . The solid lines are the corresponding spin–lattice relaxation functions, and the dashed lines are fits with eq 8.

time constant  $\tau$  of the slower process is compared with that obtained from fitting to a single peak function at higher temperatures. We see that all data are well described by a VFT behavior,<sup>34–36</sup>  $\tau = \tau_0 \exp[DT_0/(T - T_0)]$ , with  $\log(\tau_0/\text{s}) = -14.3 \pm 0.4$ ,  $D = 15 \pm 2$ , and  $T_0 = 104 \pm 2 \text{ K}$ .

**$^2\text{H}$  NMR Experiments.** Figure 5 shows  $^2\text{H}$  spin–lattice relaxation times reflecting the water dynamics in the mixture. The mean spin–lattice relaxation times  $\langle T_1 \rangle$  are displayed to take into account a nonexponential buildup of the magnetization at low temperatures (see below). Due to interfering effects of crystallization, we were not able to perform NMR studies of the supercooled state in the temperature range of ca. 170–200 K. We see that  $\langle T_1 \rangle$  displays a minimum at  $1000/T = 4.4 \text{ K}^{-1}$  (227 K). The minimum value  $\langle T_1 \rangle_{\text{min}} = 1.9 \text{ ms}$  is larger than the value of 1.4 ms expected for a Debye spectral density. This deviation indicates that the water dynamics is not described by an exponential correlation function. Therefore, we use the CC (eq 4) and the CD (eq 5) spectral densities for further analysis, as they proved to be useful in various spin–lattice relaxation studies of nonexponential molecular dynamics.<sup>22</sup> Then, the width parameters  $\beta_{\text{CC}}$  and  $\beta_{\text{CD}}$  can be determined from the value of  $\langle T_1 \rangle_{\text{min}}$ . The analysis yields  $\beta_{\text{CC}} = 0.80$  and  $\beta_{\text{CD}} = 0.53$ , implying that the width of the underlying distribution  $G(\log \tau)$  is moderate. For example, we found substantially smaller values,  $\beta_{\text{CC}} = 0.45$ – $0.50$  and  $\beta_{\text{CD}} = 0.19$ – $0.22$ , for the hydration water of proteins.<sup>10,14</sup> We assume that the width of the distribution  $G(\log \tau)$  and, thus, the parameters  $\beta_{\text{CC}}$  and  $\beta_{\text{CD}}$  do not depend on temperature in a relatively narrow temperature range around the  $\langle T_1 \rangle$  minimum, allowing us to determine the rotational correlation times  $\tau_{\text{CC}}$  and  $\tau_{\text{CD}}$ . In Figure 4, we see that the resulting values of  $\tau_{\text{CC}}$  and  $\tau_{\text{CD}}$  are virtually identical. Moreover, it is evident that the present data agree well with rotational correlation times reported for a similar mixture in a previous  $^1\text{H}$  spin–lattice relaxation study,<sup>38</sup> which assumed a Debye spectral density. These findings mean that, due to the moderate non-exponentiality, the choice of the spectral density is not critical when restricting the analysis to data in the vicinity of the  $\langle T_1 \rangle$  minimum. Hence, the  $^2\text{H}$  spin–lattice relaxation analysis yields reliable correlation times of water dynamics in this temperature range.

The stretching parameter  $\beta_{T_1}$  of the  $^2\text{H}$  spin–lattice relaxation function is displayed in the inset of Figure 5. We see that  $\beta_{T_1} \approx 1$  down to about  $1000/T = 6.5 \text{ K}^{-1}$  (154 K), while the stretching parameter becomes smaller when the temperature is further decreased. Hence, below 154 K, water subensembles with different dynamical behaviors exist, leading to a diversity of

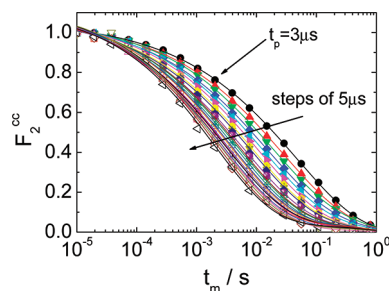


**Figure 7.** Correlation functions  $F_2^{cc}(t_m)$  measured for various evolution times in the range  $t_p = 3$ – $120 \mu\text{s}$  at  $T = 149.9 \text{ K}$ . The data are normalized to the value at the shortest mixing time  $t_m = 10^{-5} \text{ s}$ . The lines are fits with eq 8.

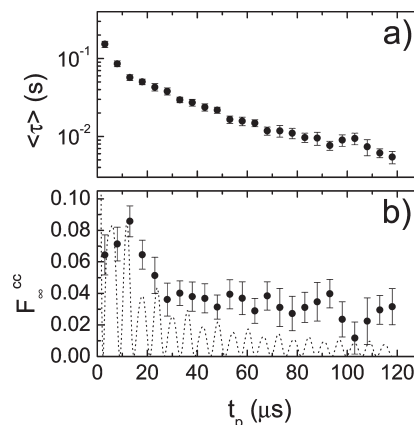


**Figure 8.** Mean correlation times  $\langle \tau \rangle$  and residual correlations  $F_2^{cc}$  resulting from interpolations of the correlation functions  $F_2^{cc}(t_m, t_p)$  in Figure 7 ( $T = 149.9 \text{ K}$ ). The dotted line in panel b corresponds to the expectation for isotropic rotational motion.

spin–lattice relaxation times  $T_1$  and, thus, to a nonexponential buildup of magnetization. This possibility of identifying different dynamical behaviors means that the water molecules do not probe the entire set of available environments on the time scale of the spin–lattice relaxation (1–20 s). At higher temperatures, the exchange of the environments and, correspondingly, of the correlation times, is sufficiently fast to establish a common spin–lattice relaxation behavior, i.e., a single relaxation time  $T_1$ , resulting in  $\beta_{T_1} = 1$ . This behavior  $\beta_{T_1}(T)$  resembles that found for the  $\alpha$  process of neat glass-forming liquids.<sup>21,24</sup>

NMR stimulated-echo analysis allows us to determine correlation times of water dynamics in the deeply supercooled mixture. The correlation functions  $f_2(t_m)$  together with the corresponding mean rotational correlation times  $\langle \tau_2 \rangle$  and stretching parameters  $\beta_2$  are obtained from  $F_2^{ss}(t_m)$  for a short evolution time of  $t_p = 3 \mu\text{s}$  (see eq 7). In Figure 6, we see that the decays of  $F_2^{ss}(t_m, t_p = 3 \mu\text{s})$  are nonexponential and shift to longer times upon cooling. Comparison with the corresponding spin–lattice relaxation functions reveals that the stimulated-echo decays are dominated by water dynamics at all studied temperatures. Following the above-described fitting approach, we interpolate the data with eq 8. The resulting stretching parameter  $\beta_2$  is temperature independent with a mean value and a standard deviation of  $\beta_2 = 0.37 \pm 0.02$ . The mean correlation times  $\langle \tau_2 \rangle = \langle \tau^s \rangle(t_p = 3 \mu\text{s})$  are included in Figure 4. As will be discussed in more detail below,

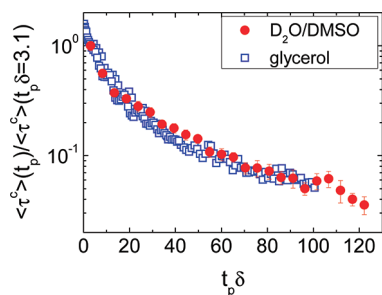


**Figure 9.** Mean rotational correlation times  $\langle \tau^c \rangle$  of molecular dynamics in supercooled liquids as a function of the scaled evolution time  $t_p \delta$ : results for water in a 2:1 molar  $D_2O/DMSO$  mixture and for neat glycerol<sup>29</sup> are compared. For glycerol, an anisotropy parameter of  $\delta = 2\pi \cdot 126$  kHz was used for the scaling.<sup>29</sup> The correlation times were scaled so as to agree at  $t_p \delta = 3.1$ .

$\langle \tau_2 \rangle$  is substantially shorter than the time constant resulting from the main dielectric relaxation peak.

To obtain information about the mechanism for water rotational motion, we analyze the dependence of  $F_2^{cc}(t_m)$  on the value of the evolution times  $t_p$  at  $T = 149.9$  K. In Figure 7, we see that  $F_2^{cc}(t_m)$  decays faster for longer evolution times, indicating that the rotational motion involves small-angle jumps.<sup>21</sup> For a quantitative analysis, we fit the data with eq 8, again using the parameters of the spin–lattice relaxation contribution determined in independent measurements.

The resulting stretching parameters  $\beta^c = 0.40 \pm 0.02$  (not shown) are independent of the length of the evolution time and consistent with that found for  $F_2^{ss}(t_m, t_p \rightarrow 0)$ . In Figure 8a, it is evident that the mean correlation times  $\langle \tau^c \rangle$  calculated from the fit parameters according to eq 9 decrease by more than an order of magnitude with increasing  $t_p$ . In general, the mean jump angle  $\langle \psi \rangle$  of molecular rotational jumps can be determined when comparing the time constants  $\tau$  for the limits  $t_p \rightarrow 0$  and  $t_p \rightarrow \infty$ .<sup>39</sup>

$$\frac{2}{3} \frac{1}{\sin^2 \langle \psi \rangle} = \frac{\tau(t_p \rightarrow 0)}{\tau(t_p \rightarrow \infty)}$$

Here, we approximate  $\tau(t_p \rightarrow 0)$  by  $\langle \tau^c(t_p = 3 \mu s) \rangle$  and  $\tau(t_p \rightarrow \infty)$  by  $\langle \tau^c(t_p = 118 \mu s) \rangle$ , yielding an *upper limit* for the mean reorientation angle of  $\langle \psi \rangle = 13^\circ$ . In Figure 4, we see that  $\langle \tau^c(t_p = 3 \mu s) \rangle \approx \langle \tau^s(t_p = 3 \mu s) \rangle$ , supporting our analyses. In particular, this agreement shows that reliable correlation times can be determined from our measurements of  $F_2^{ss}$ , although the above-described data analysis neglects the fact that the relaxation behavior of alignment order existing during the mixing time of this experiment somewhat differs from that of Zeeman order, which is observed in spin–lattice relaxation measurements.

In Figure 9, the present correlation times of water dynamics are compared with accordingly scaled literature data  $\langle \tau^c(t_p) \rangle$  reported for deeply supercooled glycerol.<sup>29</sup> Both data sets are shown as a function of  $t_p \delta$  to account for the different anisotropy parameters  $\delta$  of the deuterons in the water and glycerol molecules. A similar evolution time dependence is evident. Hence, the mechanism for the rotational motion of water in the  $D_2O/DMSO$  mixture highly resembles that for neat glycerol. Detailed analysis of the glycerol data revealed that the distribution of jump angles comprises small and large angles.<sup>29</sup> Specifically, the results for glycerol were successfully reproduced assuming a bimodal “distribution dominated by  $2^\circ$  jump angles,

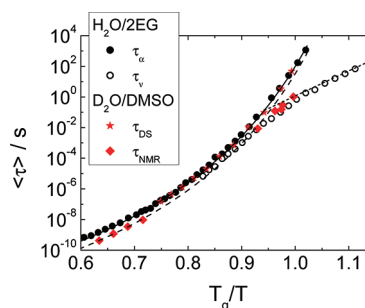


**Figure 10.** Mean time constants of molecular dynamics in two aqueous mixtures as a function of  $T_g/T$ . The present DS and NMR data for a  $D_2O/DMSO$  mixture (see Figure 4) are compared with DS results for the  $\alpha$  process and the secondary process of a mixture of water and diethylene glycol (35 wt %).<sup>42</sup> In the latter case, we used  $T_g = 154$  K, as obtained from the criterion  $\tau_\alpha(T_g) = 100$  s. The solid line corresponds to the VFT fit in Figure 4. The dashed line is the VFT fit divided by a factor of 3. The dotted line has a slope of 0.5 eV.

with 2% of  $30^\circ$  jump angles added”.<sup>29</sup> Based on the good agreement of the data in Figure 9, we conclude that the elementary rotational steps of the water molecules in the  $D_2O/DMSO$  mixture are characterized by a similar distribution of jump angles.

The residual correlation  $F_2^{cc}(t_p) = F_2^{cc}(t_m \rightarrow \infty, t_p)$  is displayed in Figure 8b. We see that water dynamics is characterized by a plateau value of  $F_\infty^{cc}(t_p \geq 60 \mu s) \approx 0.03$ , which is small, but still slightly higher than expected for isotropic reorientation. While such a deviation is difficult to reconcile with the  $\alpha$  process of a structurally and dynamically homogeneous system, such behavior would result if water exhibited a dynamical process that is faster than the  $\alpha$  process of the mixture and that involves somewhat preferred orientations with respect to DMSO or other  $D_2O$  molecules. Since the observed water reorientation is indeed faster than the  $\alpha$  process of the mixture (see Figure 4) our findings for the residual correlation suggest that a slightly anisotropic secondary relaxation exists in the studied mixture near  $T_g$ .

## DISCUSSION

We begin the discussion by drawing the reader’s attention again to Figure 4. The relaxation times obtained from the main dielectric loss peak of the studied 2:1 molar  $D_2O/DMSO$  mixture exhibit VFT temperature dependence, typical of the majority of supercooled liquids. In the low-temperature range, the dielectric data nicely agree with the relaxation time estimated from differential scanning calorimetry,<sup>37</sup> showing that the main peak of the dielectric spectra is related to the relaxation process involved in the glass transition. The extrapolation of this VFT behavior to higher temperatures deviates somewhat from the NMR correlation times in the range  $1000 \text{ K}/T = 4.25\text{--}5$ . In Figure 10, we see that a better agreement is obtained when the VFT extrapolation is divided by a factor of 3. Considering that DS and NMR probe the rotational autocorrelation functions  $f_1(t)$  and  $f_2(t)$ , respectively, an agreement of the correlation times is not expected in the general case. For example, DS and NMR correlation times differ by a factor of 3 for isotropic rotational diffusion if dynamical exchange is neglected,<sup>39–41</sup> consistent with the present results. In any case, recalling that both molecular species contribute to the dielectric signal, the temperature independence of both the shape of the dielectric loss and of



the ratio of DS and NMR correlation times indicates that D<sub>2</sub>O and DMSO dynamics are coupled down to about 170 K. Moreover, for the studied mixture, our results rule out the existence of a sharp fragile-to-strong transition at about 220 K,<sup>7</sup> which is a matter of controversial debate for aqueous systems in the literature.

While the dynamics of DMSO and D<sub>2</sub>O are coupled in most of the supercooled range, they diverge at low temperatures. Specifically, for  $T \leq 165$  K, the NMR time constants separate from the DS time constants upon cooling so that the former are almost 2 orders of magnitude shorter in the vicinity of  $T_g$  (see Figures 4 and 10). Since the correlation time of  $f_1(t)$  cannot be larger than that of  $f_2(t)$  by more than a factor of 3 if the same dynamical process is probed,<sup>39</sup> it is not possible to reconcile the NMR and DS data using such an argument. When striving for a different explanation, it is important to consider that <sup>2</sup>H NMR solely probes the water dynamics, while DS is sensitive to the dynamics of both D<sub>2</sub>O and DMSO constituents. We conclude that, in <sup>2</sup>H NMR, a dynamical process of water is observed that splits off from the  $\alpha$  process of the mixture at  $T_g/T = 0.90$ – $0.95$  and shows a milder temperature dependence. Consistently, a high-frequency shoulder of the dielectric loss peak indicates the existence of a secondary dynamical process in the vicinity of  $T_g$ . The position of this shoulder is in harmony with the correlation time of the water process obtained in <sup>2</sup>H NMR (see Figure 3).

Comparison of the nonexponentiality of the water dynamics observed in spin–lattice relaxation and stimulated-echo experiments provides further evidence that <sup>2</sup>H NMR probes different dynamical processes in the weakly and deeply supercooled mixture. At  $T_g/T = 0.9$ – $1.0$ , stimulated-echo analysis revealed strongly nonexponential correlation functions of water reorientation, which are characterized by a KWW stretching parameter of  $\beta_2 \approx 0.38$ . At  $T_g/T \approx 0.7$ , spin–lattice relaxation analysis yielded  $\beta_{CD} = 0.53$  for the width parameter of the CD distribution. Employing the relation  $\beta_{KWW} = 0.97\beta_{CD} + 0.144$ ,<sup>43</sup> this CD width parameter can be translated into a KWW stretching parameter of  $\beta_{KWW} = 0.66$ , which is significantly larger than the  $\beta_2 \equiv \beta_{KWW} \approx 0.38$  resulting from the stimulated-echo analysis. By contrast, in a <sup>2</sup>H NMR study of the  $\alpha$  process of ortho-terphenyl, consistent values of the stretching parameter were obtained in spin–lattice and stimulated-echo analyses in the weakly and deeply supercooled regime, respectively,<sup>44</sup> consistent with time–temperature superposition. Therefore, we conclude that the present stimulated-echo experiments probe a dynamical process of water that is faster and more nonexponential than the  $\alpha$  process of the D<sub>2</sub>O/DMSO mixture. However, the nonexponentiality of the observed water motion is still weaker than that of water dynamics in essentially rigid elastin and collagen matrices, which is characterized by  $\beta_2 \equiv \beta_{KWW} \approx 0.28$ .<sup>10</sup>

In Figure 10, we compare the relaxation times of two aqueous mixtures exhibiting comparable glass transition temperatures. Specifically, we plot the present data together with literature data for 35 wt % of water in diethylene glycol.<sup>42</sup> Evidently, on a  $T_g/T$  scale, the temperature dependence of the  $\alpha$  process of both mixtures is virtually identical. In addition, a faster relaxation exhibiting a weaker temperature dependence and separation from the  $\alpha$  process upon cooling is observed for the water/diethylene glycol mixture. The time constant of this faster relaxation agrees well with that of the faster dynamical process of water found in the present approach. Such secondary

relaxation was reported for various aqueous solutions and argued to originate from the water component.<sup>1–3,45</sup> Although we cannot completely rule out the possibility that the water reorientation probed in the present <sup>2</sup>H NMR stimulated-echo experiments is specific to our sample, we conclude that the D<sub>2</sub>O/DMSO mixture belongs to the group of systems featuring this “universal” water-specific secondary relaxation, which was referred to as the  $\nu$  process by some authors.<sup>1,46</sup>

The present <sup>2</sup>H NMR stimulated-echo experiments provide detailed insights into the geometry of the water reorientation underlying this secondary relaxation in the supercooled liquid regime. For the studied D<sub>2</sub>O/DMSO mixture at  $0.9 < T_g/T \leq 1.0$ , we found that the rotational autocorrelation functions of this water process decay to a small residual correlation below, say, 4%. Hence, during the secondary relaxation, the water molecules cover a large solid angle, and the anisotropy of their rotational motion, if it exists, is weak. Moreover, we exploited the fact that the elementary jump angle of the reorientation process can be determined when varying the evolution time  $t_p$  and, thus, the angular resolution of the stimulated-echo experiment. The observation of a significant dependence of the mean correlation time on the evolution time,  $\langle \tau(t_p) \rangle$ , showed that small-angle jumps are an important aspect of the secondary water process in the D<sub>2</sub>O/DMSO mixture at  $T > T_g$ . Specifically, we found that the upper limit of the mean elementary jump angle amounts to 13°. Our findings for  $\langle \tau(t_p) \rangle$  resemble results for various highly viscous molecular and polymeric liquids in the vicinity of  $T_g$ .<sup>21,29,41,47,48</sup> By contrast,  $\langle \tau \rangle$  was observed to be independent of  $t_p$  in our previous <sup>2</sup>H NMR works on water rotational motion in rigid protein matrices at  $T < 200$  K,<sup>10,15,49</sup> indicating jump angles on the order of the tetrahedral angle. Large-angle jumps were also found for the motion of water in molecular dynamics simulations of water–protein mixtures at sufficiently low temperatures<sup>50</sup> and for the reorientation of small guest molecules in glassy polymer matrices.<sup>51–53</sup> Thus, comparison of our present and previous findings implies that the mechanism for the water-specific secondary relaxation depends on the viscosity of the environment. In particular, rotational jumps of water about small angles and large angles dominate above and below  $T_g$ , respectively.

We proceed by discussing the present findings in the context of previous results for water dynamics in mixtures and confinements. In various matrices, the temperature-dependent correlation times of water dynamics were found to show a crossover from non-Arrhenius to Arrhenius behavior upon cooling. However, the origin and the temperature of such crossover are still the subject of controversial debate. The conjecture of a fragile-to-strong transition at ca. 220 K,<sup>7</sup> implying that the  $\alpha$  process is observed both above and below the crossover, does not explain the findings for the present aqueous mixture, as was discussed above. Another rationale for a kink in temperature-dependent correlation times is the argument that primary and secondary relaxations are observed at sufficiently high and low temperatures, respectively.<sup>1–4,9,10,45,46</sup> While some authors argued that a crossover is induced by confinement,<sup>2,54</sup> others regard such phenomenon as an intrinsic property of water.<sup>55</sup> Specifically, in the confinement scenario,<sup>2,54</sup> the increase of the cooperativity of water dynamics upon cooling and, thus, of the temperature dependence of the relaxation times, was argued to stop when the cooperative length scale becomes comparable to the size of a confinement, which can be produced by a porous material or by a glassy matrix. In the intrinsic scenario, ice-like relaxation

processes are proposed to set in when the tetrahedral network structure of water is completed. Moreover, the hypothesis was put forward that the secondary relaxation of aqueous systems denoted as the  $\nu$  process can be identified with the Johari–Goldstein (JG)  $\beta$  process of water.<sup>1,45</sup> Then, as one of the universal properties of the JG  $\beta$  process, a crossover in the temperature dependence is expected to occur at  $T_g$ .<sup>1,45</sup> In addition, a second crossover resulting from an  $\alpha$ – $\beta$  splitting can exist at  $T_s > T_g$ .<sup>56</sup> Specifically, the temperature dependence will change at the splitting temperature if the  $\beta$  process dominates the experimental findings below the splitting.

The present findings are in harmony with a crossover in the temperature dependence due to an  $\alpha$ – $\nu$  splitting at a temperature  $T_s > T_g$ . Consistent with this conclusion, we find a change of the temperature dependence in the deeply supercooled regime and, hence, the effect is different from the above-mentioned crossover of secondary relaxations at  $T = T_g$ . However, our results do not exclude that the temperature-dependent correlation times show another kink when further cooling through the glass transition, but they rather leave room for the existence of such effect. Specifically, the temperature dependence observed in the present stimulated-echo study is substantially higher than that expected based on the widely universal activation energy of 0.5 eV for low-temperature water dynamics,<sup>2,57</sup> suggesting that there might be another crossover at a lower temperature (see Figure 10). Below  $T_s$ , the water molecules cover a large solid angle during the secondary relaxation so that the  $\nu$  process destroys essentially all orientational correlation, hampering an observation of the  $\alpha$  process of water in stimulated-echo experiments in the vicinity of  $T_g$ . However, the  $\alpha$  process of water can still exist in this temperature range. Actually, the water molecules must be involved in the flow process of the liquid, and the observation of a single glass transition step implies that there is a common  $\alpha$  process of D<sub>2</sub>O and DMSO molecules, as was previously argued for hydrogen-bonded mixtures.<sup>45</sup> Thus, we propose that two water processes exist in the deeply supercooled D<sub>2</sub>O/DMSO mixture. Comparison with results for other aqueous mixtures suggests that the slower of these processes is the  $\alpha$  process, while the faster is the secondary  $\nu$  relaxation of water.

To sum up the discussion, we point out two important conclusions of this study: first, the mechanism of the  $\nu$  process in the viscous mixture (D<sub>2</sub>O/DMSO,  $T_s > T > T_g$ ) differs from that for water in frozen matrices (water/protein,  $T_g > T$ ), but it resembles that found for neat glass-forming liquids at temperatures slightly above  $T_g$ . While the findings for neat systems were attributed to the main relaxation process, the  $\alpha$  process, we found evidence that the present results are related to a secondary relaxation of the studied mixture, the  $\nu$  process. Second, the  $\alpha$ – $\nu$  splitting observed in the temperature dependence of the time constants in this study resembles the  $\alpha$ – $\beta$  splitting observed in neat glass formers. However, it should be noted that the present  $\alpha$ – $\nu$  splitting occurs at  $\tau \approx 10^{-2}$  s, while the JG  $\beta$  process usually separates from the  $\alpha$  process at  $\tau$  within the range  $10^{-5}$  to  $10^{-7}$  s.<sup>58</sup> Recently, it was shown that the time constant of the low-temperature water process exponentially decreases with the weight fraction of water,<sup>3</sup> suggesting that the nature of water dynamics depends on not only the flexibility of the environment, but also the size of water clusters. Moreover, there is another important difference between the phenomenology of the JG  $\beta$  process of neat glass formers and that of the  $\nu$  process of aqueous mixtures: the activation energy of the JG  $\beta$  process is related to the value of the glass transition temperature, e.g.,  $E_a = 24 T_g$ <sup>59</sup> is

found for a number of glass formers, while the temperature dependence of the  $\nu$  process is characterized by a widely universal value of  $E_a = 0.5$  eV, independent of the glass transition temperature of the aqueous mixture.<sup>2,57</sup> Finally, it should be noted that small-amplitude rotational motions are associated with the JG  $\beta$  process of van der Waals glass formers below  $T_g$ ,<sup>60–62</sup> while the  $\nu$  process of water displays large-amplitude rotational motion at  $T < T_g$ .<sup>10,14,15</sup> With these reservations, the possibility arises to identify the  $\nu$  process in the D<sub>2</sub>O/DMSO mixture with the JG  $\beta$  process. Then, the similarities of the mechanisms for the  $\nu$  process and for the  $\alpha$  process of neat systems lead back to the long-standing question of whether the JG  $\beta$  process is the elementary relaxation step of the  $\alpha$  process, and, at the same time, they pose the question of whether it is possible to discuss the relaxation processes of neat and mixed glass-forming liquids on common grounds. Future combined <sup>2</sup>H NMR and DS studies of water dynamics in mixtures should shed light on the questions of whether the mechanism for water reorientation differs in matrices of diverse rigidity and to what extent the  $\nu$  process can be identified with the JG  $\beta$  process.

## AUTHOR INFORMATION

### Corresponding Author

\*E-mail address: michael.vogel@tu-darmstadt.de.

## ACKNOWLEDGMENT

We thank R. Böhmer, TU Dortmund, for helpful comments on the manuscript.

## REFERENCES

- (1) Capaccioli, S.; Ngai, K. L.; Shinyashiki, N. *J. Phys. Chem. B* **2007**, *111*, 8197–8209.
- (2) Cervený, S.; Alegria, A.; Colmenero, J. *Phys. Rev. E* **2008**, *77*, 031803.
- (3) Sjöström, J.; Mattsson, J.; Bergman, R.; Johansson, E.; Josefsson, K.; Svantesson, D.; Swenson, J. *Phys. Chem. Chem. Phys.* **2010**, *12*, 10452–10456.
- (4) Swenson, J.; Jansson, H.; Bergman, R. *Phys. Rev. Lett.* **2006**, *96*, 247802.
- (5) Angell, C. A. *Chem. Rev.* **2002**, *102*, 2627–2650.
- (6) Angell, C. A. *Science* **2008**, *319*, 582–587.
- (7) Chen, S. H.; Liu, L.; Fratini, E.; Baglioni, P.; Faraone, A.; Mamontov, E. *Proc. Natl. Acad. Sci. U.S.A.* **2006**, *103*, 9012–9016.
- (8) Kumar, P.; Franzese, G.; Stanley, H. E. *J. Phys.: Condens. Matter* **2008**, *20*, 244114.
- (9) Pawlus, S.; Khodadadi, S.; Sokolov, A. P. *Phys. Rev. Lett.* **2008**, *100*, 108103.
- (10) Vogel, M. *Phys. Rev. Lett.* **2008**, *101*, 225701.
- (11) Gainaru, C.; Fillmer, A.; Böhmer, R. *J. Phys. Chem. B* **2009**, *113*, 12628–12631.
- (12) Doster, W.; Busch, S.; Gaspar, A. M.; Appavou, A.-S.; Wuttke, J.; Scheer, H. *Phys. Rev. Lett.* **2010**, *104*, 098101.
- (13) Khodadadi, S.; Pawlus, S.; Sokolov, A. P. *J. Phys. Chem. B* **2008**, *112*, 14273–14280.
- (14) Lusceac, S. A.; Vogel, M. R.; Herbers, C. R. *Biochim. Biophys. Acta, Proteins Proteomics* **2010**, *1804*, 41–48.
- (15) Lusceac, S. A.; Vogel, M. *J. Chem. Phys. B* **2010**, *114*, 10209–10216.
- (16) Lusceac, S. A.; Rosenstihl, M.; Vogel, M.; Gainaru, C.; Fillmer, A.; Böhmer, R. *J. Non-Cryst. Solids* **2011**, *357*, 655–663.
- (17) Böttcher, C. I. F.; Borderwijk, P. *Theory of Electric Polarization*; Elsevier: Amsterdam, 1978; Vol. 2.
- (18) Havriliak, S.; Negami, S. *Polymer* **1967**, *8*, 161.



- (19) Schmidt-Rohr, K.; Spiess, H. W. *Multidimensional Solid-State NMR and Polymers*; Academic Press: New York, 1994.
- (20) Bloembergen, N.; Purcell, E. M.; Pound, R. V. *Phys. Rev.* **1948**, *73*, 679–712.
- (21) Böhmer, R.; Diezemann, G.; Hinze, G.; Rössler, E. *Prog. Nucl. Magn. Reson. Spectrosc.* **2001**, *39*, 191–267.
- (22) Beckmann, P. A. *Phys. Rep.* **1988**, *171*, 85–128.
- (23) Rössler, E.; Sillescu, H. *Chem. Phys. Lett.* **1984**, *16*, 327–336.
- (24) Schnauss, W.; Fujara, F.; Sillescu, H. *J. Chem. Phys.* **1992**, *97*, 1378.
- (25) Williams, G.; Watts, D. C. *Trans. Faraday Soc.* **1970**, *66*, 80.
- (26) Spiess, H. W. *J. Chem. Phys.* **1980**, *72*, 6755.
- (27) Müller, A.; Zimmermann, H.; Haeberlen, U. *J. Magn. Reson.* **1997**, *126*, 66.
- (28) Fujara, F.; Geil, B.; Sillescu, H.; Fleischer, G. *Z. Phys. B* **1992**, *88*, 195.
- (29) Böhmer, R.; Hinze, G. *J. Chem. Phys.* **1998**, *109*, 241.
- (30) Wagner, H.; Richert, R. *J. Phys. Chem.* **1999**, *103*, 4071.
- (31) Dreizler, H.; Dendl, G. *Z. Naturforsch. Pt. A* **1964**, *A19*, 512.
- (32) Clough, S. A.; Beers, Y.; Klein, G. P.; Rothman, L. S. *J. Chem. Phys.* **1973**, *59*, 2254.
- (33) Schaefer, D.; Leisen, J.; Spiess, H. W. *J. Magn. Reson.* **1995**, *115*, 60–79.
- (34) Vogel, H. *Phys. Z.* **1921**, *22*, 645.
- (35) Fulcher, G. S. *J. Am. Ceram. Soc.* **1925**, *8*, 339.
- (36) Tammann, G.; Hesse, G. *Z. Anorg. Allg. Chem.* **1926**, *156*, 245.
- (37) Rasmussen, D. H.; MacKenzie, A. P. *Nature* **1968**, *220*, 1315–1317.
- (38) Parker, K. J.; Tomlinson, D. J. *T. Faraday Soc.* **1971**, *67*, 1302–1314.
- (39) Anderson, J. E. *Faraday Symp. Chem. Soc.* **1972**, *6*, 82.
- (40) Ivanov, E. N. *Sov. Phys. JETP* **1964**, *18*, 1041.
- (41) Diezemann, G.; Böhmer, R.; Hinze, G.; Sillescu, H. *J. Non-Cryst. Solids* **1998**, *235–237*, 121.
- (42) Sudo, S.; Tsubotani, S.; Shimomura, M.; Shinyashiki, N. *J. Chem. Phys.* **2004**, *121*, 7332–7340.
- (43) Lindsey, C. P.; Patterson, G. D. *J. Chem. Phys.* **1980**, *73*, 3348–3357.
- (44) Dries, T.; Fujara, F.; Kiebel, M.; Rössler, E.; Sillescu, H. *J. Chem. Phys.* **1988**, *88*, 2139–2147.
- (45) Capaccioli, S.; Ngai, K. L.; Ancherbak, S.; Rolla, P. A.; Shinyashiki, N. *J. Non-Cryst. Solids* **2011**, *357*, 641–654.
- (46) Shinyashiki, N.; Sudo, S.; Yagihara, S.; Spanoudaki, A.; Kyritsis, A.; Pissis, P. *J. Phys.: Condens. Matter* **2007**, *19*, 205113.
- (47) Vogel, M.; Torbrügge, T. *J. Chem. Phys.* **2006**, *125*, 164910.
- (48) Tracht, U.; Heuer, A.; Spiess, H. W. *J. Chem. Phys.* **1999**, *111*, 3720–3727.
- (49) Vogel, M. *Eur. Phys. J. Spec. Top.* **2010**, *189*, 47–64.
- (50) Vogel, M. *J. Phys. Chem. B* **2009**, *113*, 9386–9392.
- (51) Vogel, M.; Rössler, E. *J. Phys. Chem. A* **1998**, *102*, 2102–2108.
- (52) Medick, P.; Vogel, M.; Rössler, E. *J. Magn. Reson.* **2002**, *159*, 126–136.
- (53) Vogel, M.; Medick, P.; Rössler, E. *Annu. Rep. NMR Spectrosc.* **2005**, *56*, 231–299.
- (54) Cervený, S.; Barroso-Bujans, F.; Alegria, A.; Colmenero, J. *J. Phys. Chem. C* **2010**, *114*, 2604–2612.
- (55) Swenson, J.; Teixeira, J. *J. Chem. Phys.* **2010**, *132*, 014508.
- (56) Paluch, M.; Roland, C. M.; Pawlus, S.; Ziolo, J.; Ngai, K. L. *Phys. Rev. Lett.* **2003**, *91*, 115701.
- (57) Cervený, S.; Schwartz, G. A.; Bergman, R.; Swenson, J. *Phys. Rev. Lett.* **2004**, *93*, 245702.
- (58) Hansen, C.; Stickel, F.; Berger, T.; Richert, R.; Fischer, E. W. *J. Chem. Phys.* **1997**, *107*, 1086–1093.
- (59) Kudlik, A.; Tschirwitz, C.; Benkhof, S.; Blochowicz, T.; Rössler, E. *Europhys. Lett.* **1997**, *40*, 649–645.
- (60) Vogel, M.; Rössler, E. *J. Phys. Chem. B* **2000**, *104*, 4285–4287.
- (61) Vogel, M.; Rössler, E. *J. Chem. Phys.* **2001**, *114*, 5802–5815.
- (62) Vogel, M.; Rössler, E. *J. Chem. Phys.* **2001**, *115*, 10883–10891.